RMetS
Royal Meteorological Society

Quantifying air temperature evolution in the permafrost region from 1901 to 2014

Donglin Guo,[a,b,c]* Duo Li[d,e] and Wei Hua[c]

[a] *Nansen-Zhu International Research Center, Institute of Atmospheric Physics, Chinese Academy of Sciences, Beijing, China*
[b] *Collaborative Innovation Center on Forecast and Evaluation of Meteorological Disasters (CIC-FEMD), Nanjing University of Information Science and Technology, China*
[c] *School of Atmospheric Sciences/Joint Laboratory of Climate and Environment Change, Chengdu University of Information Technology, China*
[d] *National Climate Center, China Meteorological Administration, Beijing, China*
[e] *Key Laboratory of Tibetan Environment Changes and Land Surface Processes, Institute of Tibetan Plateau Research, Chinese Academy of Sciences, Beijing, China*

ABSTRACT: Permafrost is sensitive to climate change. In recent decades, a growing body of research has focused mainly on the study of permafrost thaw, but leaving the climate change in the permafrost region that has not been adequately assessed, which is of first importance for the research on permafrost thaw. Using gridded observations from the Climatic Research Unit (CRU), in conjunction with the European Centre for Medium-Range Weather Forecasts Reanalysis Interim (ERA-Interim) and Japanese 55-year Reanalysis (JRA-55) data, this study investigates characteristics of air temperature evolution in the region of permafrost throughout the 20th century. Results show that yearly air temperatures in the permafrost region of the Northern Hemisphere experienced a statistically significant warming, with trends of $0.13\,°C\,decade^{-1}$ for 1901–2014 and $0.40\,°C\,decade^{-1}$ for 1979–2014. Winter air temperatures showed the greatest increase during 1901–2014, while autumn air temperatures increased the most during 1979–2014. In addition, increases in air temperature in high-latitude permafrost sub-region are greater than those in high-elevation permafrost sub-region, and air temperatures in the permafrost sub-region of Mongolia have the largest trend from 1901 to 2014, followed by those in Russia, Alaska, Canada, and China. Air temperatures in the permafrost region increased 1.7 times more than temperatures globally from 1901 to 2014, and underwent an increase at a rate of $0.32\,°C\,decade^{-1}$ during the period 1998–2014, when the global warming hiatus occurred with a trend of $0.06\,°C\,decade^{-1}$. This implies that permafrost thaw may have continued during the global warming hiatus period. The close agreement between CRU data and ERA-Interim and JRA-55 reanalysis data indicates good reliability of air temperature evolution characteristics. These results provide information relevant to climate change in the permafrost region, and are useful for researching and understanding historical permafrost change.

KEY WORDS   air temperature; permafrost region; permafrost thaw; CRU

Received 24 October 2016; Revised 25 February 2017; Accepted 11 May 2017

1. Introduction

Permafrost is defined as earth materials that remain at (or below) 0 °C for at least two consecutive years (Muller, 1947). Permafrost is mostly distributed in high-latitude and high-elevation regions in the Northern/Southern Hemisphere. According to an estimate from Zhang *et al.* (1999), the Northern Hemisphere has a permafrost area of approximately $22.8 \times 10^6\,km^2$, which is equivalent to approximately 25% of the land area in the Northern Hemisphere (Zhang *et al.*, 1999). Defined as a function of ground temperature, permafrost is sensitive to climate change (Romanovsky *et al.*, 2010a; Yang *et al.*, 2010); therefore, if the global climate warms, permafrost may undergo thawing (Romanovsky *et al.*, 2010b).

Permafrost thaw has important impacts on hydrology and water resources, climate change, ecosystems, and human infrastructure (Callaghan *et al.*, 2012). According to an estimate based on ground ice content relating to the circumpolar map of the International Permafrost Association (IPA), approximately $11.37–36.55 \times 10^3\,km^3$ of ground ice is stored in permafrost soils in the Northern Hemisphere (Zhang *et al.*, 1999). Melting of these ground ice reserves would have a considerable effect on hydrology and water resources (Lawrence and Slater, 2005; Lan *et al.*, 2015; Liljedahl *et al.*, 2016). In addition, it is estimated that approximately two times more carbon is stored in permafrost soils in boreal and Arctic ecosystems than in the current atmosphere (Zimov *et al.*, 2006; Schuur *et al.*, 2009). Therefore, climate warming would be accelerated if permafrost thaw releases this carbon (Schuur *et al.*, 2009, 2015; Koven *et al.*, 2011, 2015; Burke *et al.*, 2013). Furthermore, the seasonal freezing and thawing processes of the active layer of permafrost regulate spatiotemporal

variations in soil water and heat at, and near, the sur-face (Yang *et al.*, 2010; Guo *et al.*, 2011a, 2011b; Li and Chen, 2013; Guo and Wang, 2014; Qin *et al.*, 2014). The permafrost thawing would disturb this regulation and affect soil biogeochemical cycles, local hydrological pro-cesses, surface energy budgets, and vegetation, which are all related to soil water and heat variations in the near sur-face. In addition to these problems, the melting of ground ice in permafrost could result in settling of the ground's surface and further affect the stability of human engineer-ing facilities, which have expanded into permafrost regions in recent decades due to the economic importance of these areas (Nelson *et al.*, 2001, 2002; Anisimov and Reneva, 2006; Guo and Sun, 2015).

In relation to the considerable impacts mentioned above, a growing number of researchers have investigated permafrost thaw in recent decades (Anisimov and Nel-son, 1996; Brown *et al.*, 2000; Stendel and Christensen, 2002; Harris and Isaksen, 2008; Wu and Zhang, 2008; Christiansen *et al.*, 2010; Romanovsky *et al.*, 2010a, 2016; Smith *et al.*, 2010; Zhao *et al.*, 2010; Derksen *et al.*, 2012; Guo *et al.*, 2012; Lawrence *et al.*, 2012; Guo and Wang, 2013, 2016a, 2016b; Koven *et al.*, 2013; Slater and Lawrence, 2013; Noetzli *et al.*, 2016). In this respect, to investigate the thermal state of permafrost (TSP) and the response of the active layer to climate change, the circumpolar active layer monitoring (CALM) and international polar year (IPY)-TSP projects have been initiated and conducted. According to active layer observations from the CALM program, Shiklomanov *et al.* (2012) reported that trends in the circumpolar active layer thickness vary by region, and that an increase in the active layer thickness is found in all regions except for in Northern Alaska and Western Siberia. Based on the observations from 575 monitoring boreholes from the IPY program, Romanovsky *et al.* (2010a) reported a consider-able warming of permafrost during the past 20–30 years and that colder permafrost has experienced a faster rate of warming. In addition, using three general climate models (GCMs) and an empirical paleo-reconstruction in conjunction with a surface frozen index model, Anisimov and Nelson (1996) indicated a reduction of 25–44% in the total permafrost area in response to a 2 °C global warming scenario. Furthermore, based on outputs from the fully coupled Community Climate System Model version 4 (CCSM4), Lawrence *et al.* (2012) showed that the total area of near-surface permafrost will decrease by 33% (RCP2.6), 49% (RCP4.5), 62% (RCP6.0), or 72% (RCP8.5) by the period of 2080–2099 [representative concentration pathway (RCP)]. More recently, outputs from multiple CMIP5 models have also been employed to examine permafrost thermal dynamics and response to climate change (Koven *et al.*, 2013; Slater and Lawrence, 2013; Guo and Wang, 2016a). However, what are the characteristics of climate change in the permafrost regions that do induce permafrost changes, and what are the dif-ferences between climate changes in the permafrost region and those occurring globally? These issues are important

in researching and understanding permafrost thaw, but they have not yet been fully assessed and quantified.

Although some studies have referred to the evolution of Arctic land surface air temperature evolution (Hartmann *et al.*, 2013; Blunden and Arndt, 2016), they have only focused on the region 60°–90°N. A large portion of permafrost, i.e. permafrost in southern Russia and on the Tibetan Plateau, is located south of 60°N. Hartmann *et al.* (2013) showed that there is large spatial variability in changes in land surface air temperatures. Therefore, the evolution of air temperature in the region of per-mafrost may differ from those in the Arctic. Although some studies have referred to air temperature changes in the permafrost region and the impact of such change on permafrost (Romanovsky *et al.*, 2010a, 2010b; Smith *et al.*, 2012; Throop *et al.*, 2012), they have only been conducted using data from a small amount of meteorolog-ical stations, and thus the results generally have limited spatial representation.

The objectives of this study are to examine: (1) the yearly and seasonal evolutionary characteristics of air tem-perature in the entire permafrost region (Northern Hemi-sphere), (2) the yearly air temperature evolutions in dif-ferent sub-regions of permafrost, and (3) differences in air temperature changes between permafrost and global regions during the 20th century on a regional scale. This study uses gridded observations from the Climatic Research Unit (CRU) Time-Series 3.2.3 in combination with the European Centre for Medium-Range Weather Forecasts Reanalysis Interim (ERA-Interim) and Japanese 55-year Reanalysis (JRA-55) data.

2. Data and methods

2.1. Data

High-resolution gridded monthly air temperature observa-tions used are the latest version of the CRU Time-Series 3.2.3 produced by the CRU at the University of East Anglia (http://www.cru.uea.ac.uk/). The data cover the period 1901–2014 and have a horizontal resolution of 0.5° [0 (polar)–56 (equator) km] longitude × 0.5° (~56 km) lat-itude. The original input values used to produce the data are monthly station observations provided by the World Meteorological Organization (WMO) in conjunction with the US National Oceanographic and Atmospheric Admin-istration/National Climatic Data Center. CRU data are constructed using the climate anomaly method (Peterson *et al.*, 1998; Wu and Gao, 2013). Station anomalies are first interpolated into high-resolution grid cells and then combined with an existing climatology to obtain abso-lute values (Harris *et al.*, 2014). Compared to the previ-ous version, this latest version of CRU data includes some new stations that provide temperature and precipitation. More detailed information about CRU data can be found in Harris *et al.* (2014). As one of the best-known gridded observation datasets, CRU data have been widely used in understanding the course of climate change throughout the

period of existing record (Simmons *et al.*, 2004; Hartmann *et al.*, 2013).

Yearly HadCRUT4 global surface air temperature anomaly data are developed jointly by the Met Office Hadley Centre and the CRU (http://www.cru.uea.ac .uk/) (Jones *et al.*, 2012). These data cover the period 1880–2015 and have a resolution of 5° [0 (polar)–555 (equator) km] longitude × 5° (~555 km) latitude. In this study, these data are used to perform a comparison between air temperature change in the permafrost regions and the globe as a whole.

Monthly air temperatures from ERA-Interim and JRA-55 reanalysis data are used as a reference to evaluate the suitability of CRU data in the permafrost regions. ERA-Interim is produced by the European Centre for Medium-Range Weather Forecasts (ECMWF) using a sequential data assimilation process, in which the state of the global atmosphere and surface is estimated by observations combined with prior information from a forecast model. ERA-Interim reanalysis employs the 31r2 version of ECMWF's Integrated Forecast System, which incorporates a forecast model with three fully coupled components for the atmosphere, land surface, and ocean waves. The observations include conventional *in situ* observations and satellite data. These data cover the period from 1979 to the present, with a horizontal resolution of 0.75° [0 (polar)–83 (equator) km] longitude × 0.75° (~83 km) latitude. More details can be found in Dee *et al.* (2011). As one of the most reliable reanalysis datasets, ERA-Interim data have been widely used to understand climate variations and to drive climate models (Sylla *et al.*, 2010; Wang and Zeng, 2012; Ngo-Duc *et al.*, 2016; Zhou *et al.*, 2016).

JRA-55 data are produced by the Japan Meteorological Agency's (JMA) operational data assimilation system, which is constantly updated to ensure it is state-of-the-art. Together with the background and atmospheric forcing fields generated by a forecast model, observations are used to estimate the global atmospheric state. Observations used for assimilation use as many conventional station observations as possible and high-quality reprocessed satellite observations. The forecast model used for the assimilation is the TL319 spectral resolution version of the JMA global spectral model; this incorporates extensive improvements compared to the previous version used in JRA-25. JRA-55 data cover the last half-century from 1958 to the present and have a horizontal resolution of 1.25° [0 (polar)–139 (equator) km] longitude × 1.25° (~139 km) latitude. More detailed information can be found in Kobayashi *et al.* (2015). JRA-55 data have been widely used to assess past and current climate conditions (Guo and Wang, 2016a; Kobayashi and Iwasaki, 2016; Yanase *et al.*, 2016).

The permafrost region is examined in relation to the Circum-Arctic map of permafrost and ground ice conditions (Brown *et al.*, 1997), in which permafrost is classified as continuous, discontinuous, isolated, or sporadic (Figure 1). The map contains the most appropriate data on a global scale of present-day permafrost distribution, has a resolution of 0.5° [0 (polar)–56 (equator) km]
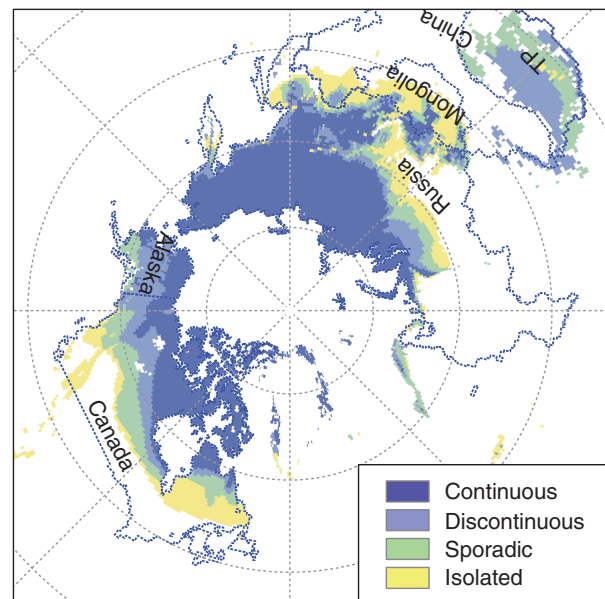

Figure 1. Distribution of different permafrost zones from the IPA map (Brown *et al.*, 1997). Five countries (states) and the Tibetan Plateau, which contain most of the permafrost, are outlined in blue dashed lines.

longitude × 0.5° (~56 km) latitude, and is archived at the website http://nsidc.org/data/.

Projected monthly air temperature data under two RCPs scenarios [RCP4.5 (an intermediate emission scenario) and RCP8.5 (a high emission scenario)] are obtained from CMIP5 simulations (http://cmip-pcmdi.llnl .gov/cmip5/) to examine future air temperature changes in the permafrost region. Twenty-one climate models are used: ACCESS1-0, bcc-csm1-1, bcc-csm1-1-m, CanESM2, CCSM4, CESM1-BGC, CESM1-CAM5, CMCC-CMS, CNRM-CM5, CSIRO-Mk3.6.0, GISS-E2-H, GISS-E2-H-CC, GISS-E2-R, GISS-E2-R-CC, INMCM4, MIROC5, MIROC-ESM, MIROC-ESM-CHEM, MRI-CGCM3, NorESM1-M, and NorESM1-ME. The basic information (e.g. resolution and reference) relating to these models is presented in Guo and Wang (2016a) and additional details with respect to simulations are provided in Taylor *et al.* (2012). These data are archived at the Earth System Grid Federation gateway (https://pcmdi.llnl.gov/) and have been widely used in evaluating future climate dynamics (Collins *et al.*, 2013).

2.2. Methods

The data listed above have different horizontal resolutions. Therefore, to perform homogenous calculations and comparisons, CRU data, ERA-Interim data, JRA-55 data, and all climate model data are interpolated to a resolution of 0.5° [0 (polar)–56 (equator) km] longitude × 0.5° (~56 km) latitude on the Circum-Arctic map of permafrost and ground ice conditions (Brown *et al.*, 1997). Similarly, as the various datasets span differing time periods, a common period (1901–2014) shared by all datasets is used to make a homogenous comparison. Furthermore, a common sub-period of 1979–2014 is also used for analysis.

In this study, the trend in air temperature is computed using the least squares fitting method to derive the slope of the linear regression with a MATLAB program. The statistical significance of the trend is evaluated in accordance with the student's t-test method.

This study investigates the evolution of air temperature in the permafrost region during the 20th century using gridded CRU observations. However, CRU data may be generally less accurate in the permafrost regions as there are relatively fewer observation stations located in such regions due to the high latitude or elevation (Way and Bonnaventure, 2015). Number of CRU stations in the permafrost regions increased from 48 in 1901 to 223 in 1964; following this date the numbers remained stable until 1989, but gradually declined to approximately 110 stations by 2014. Therefore, the fewer number of observation stations may reduce the accuracy of CRU data, despite the state-of-the-art interpolation method used to produce the data. To address this issue, we used two sets of reanalysis data (ERA-Interim and JRA-55) to validate the performance of CRU data in the permafrost regions. As the reanalysis data depend on a considerable amount of model and satellite data that generally have a relatively homogeneous performance over the entire Earth's surface, they are expected to have relatively reasonable accuracy in the permafrost regions. Therefore, they are considered suitable for evaluating the applicability of CRU data to the permafrost region. When CRU data are closer to the reanalysis data they are generally more reliable in the permafrost region.

The Nash–Sutcliffe efficiency (NSE) was developed by Nash and Sutcliffe (1970) and is used to quantitatively evaluate the level of agreement between reanalysis data and observations. The NSE is a normalized index that examines the relative magnitude of residual variance relative to the variance of the observation. It indicates how well the plot of simulations against observations fits the $1:1$ line and is sensitive to extreme values. NSE ranges from $-\infty$ to 1: an index value of 1 indicates a perfect agreement between simulation and observation, and the simulation is more accurate when the index is closer to 1. An index of less than 0 implies that the observed mean value is a better predictor than the model.

The permafrost regions can be divided into high-latitude and high-elevation permafrost sub-regions, given the different geographic characteristics that control permafrost formation (Cheng and Wang, 1982): high-latitude permafrost is controlled by latitudinal zonality and high-elevation permafrost is controlled by vertical zonality. According to this classification, as typical major high-elevation permafrost is distributed on the Tibetan Plateau, this study uses the Tibetan Plateau as a region representative of high-elevation permafrost, and the area outside the Tibetan Plateau as a region representative of high-latitude permafrost. However, despite this classification, generally, permafrost existing on some mountains (e.g. Alps) is also generally considered to be high-elevation permafrost.

Countries that possess considerable areas of permafrost are greatly concerned about its fate due to local effects of permafrost change. Therefore, the permafrost region can also be divided into sub-regions in accordance with differing countries that possess considerable areas of permafrost [Russia, Canada, Alaska (USA), Mongolia, and China]. Therefore, in this study, the temperature evolution in all sub-regions of permafrost is also analysed.

3. Results

3.1. Air temperature evolution in the entire permafrost region

Yearly temperatures in the permafrost region experienced statistically significant increases from 1901 to 2014, with a trend of $0.13\,°C\,decade^{-1}$ (Figure 2(a)) (Table 1). The increase was more significant for the period 1979–2014, with a trend of $0.39\,°C\,decade^{-1}$. Air temperatures showed an obvious increase during (approximately) the 1930s–1940s and then a decrease during (approximately) the 1950s–1960s, with an increase occurring again from the 1980s to the present. Whether or not the permafrost had an observable response to the temporary increase in air temperature during the 1930s–1940s is an issue worthy of further examination. In general, permafrost responds slowly to changes in climate (Smith $et\,al.$, 2012; Throop $et\,al.$, 2012), and therefore, examining the response of permafrost to changes in air temperature during the 1930s–1940s may help to determine what extent permafrost change lags behind changes in air temperature. The NSE between CRU data and JRA-55 and ERA-Interim reanalysis data are 0.98 and 0.96, respectively, which are very close to 1 (perfect agreement). This indicates that CRU data are suitable for application to the permafrost region and that uncertainties in the related analysis results are small.

From a seasonal perspective, CRU data show that the largest air temperature increases occurred during the winter from 1901 to 2014, with a trend of $0.18\,°C\,decade^{-1}$, followed by spring ($0.17\,°C\,decade^{-1}$), autumn ($0.09\,°C\,decade^{-1}$), and summer ($0.08\,°C\,decade^{-1}$) (Figures 2(b)–(e)). However, for the period 1979–2014, the largest increase in air temperature occurred in autumn, with a trend of $0.52\,°C\,decade^{-1}$, followed by spring ($0.48\,°C\,decade^{-1}$), and summer ($0.33\,°C\,decade^{-1}$), but winter air temperature had the lowest air temperature increase of $0.15\,°C\,decade^{-1}$. These results appear to show that winter contribute the most towards warming during 1901–2014 but the least towards warming during 1979–2014 across the four seasons. The low increase in air temperature in winter during 1979–2014, results from a negative trend in air temperature in winter in the permafrost sub-regions of Russia and Mongolia, with trends of -0.16 and $-0.11\,°C\,decade^{-1}$, respectively (Table 1). Other reasons associated with this trend may require further study. The NSE between the CRU data and JRA-55 and ERA-Interim reanalysis data range from 0.96 to 0.97 and from 0.92 to 0.97, respectively, across the four
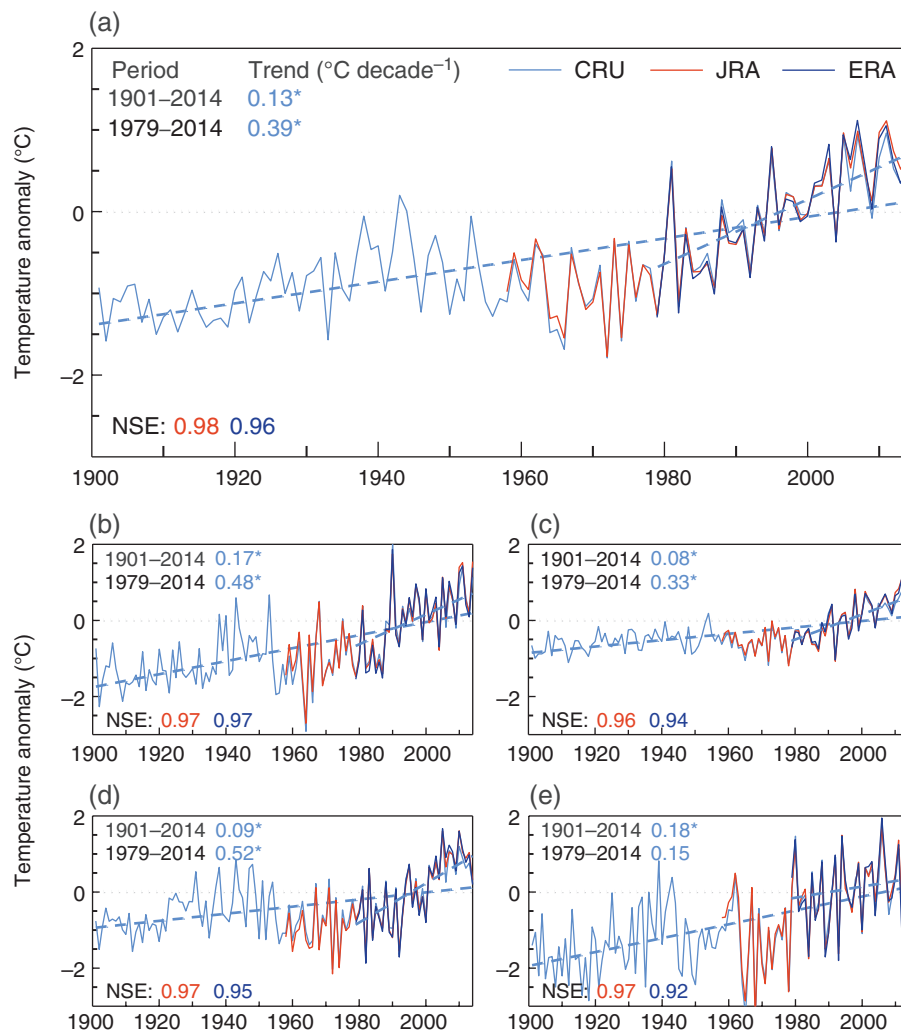
Figure 2. Changes in temperature anomalies (relative to 1981–2010) for annual (a), spring (March–April–May, MAM) (b), summer (June–July–August, JJA) (c), autumn (September–October–November, SON) (d), and winter (December–January–February, DJF) (e) over the entire permafrost region from CRU, JRA-55 (JRA), and ERA-Interim (ERA) data. Light blue lines represent regression lines of CRU temperature series for the periods 1901–2014 and 1979–2014, respectively. Temperature trends (°C decade⁻¹) from CRU data and the corresponding periods are given in the top left corner of each panel, and * indicates that trends are significant at the 95% confidence level. The NSE is given in the lower left corner of each panel to show the level of agreement between CRU observations and JRA-55 data during 1958–2014 and ERA-Interim reanalysis data during 1979–2014.

seasons. NSE values close to 1 indicate that these analysis results from the CRU data are reliable.

3.2. Air temperature evolution in differing sub-regions of permafrost

Yearly air temperatures in the high-latitude permafrost sub-region increased by 0.13 °C decade⁻¹ from 1901 to 2014; 1.63 times more than in the high-elevation permafrost sub-region, which showed an increase of 0.08 °C decade⁻¹ (Figures 3(a) and (b)) (Table 1). This greater increase in air temperature in the high-latitude permafrost sub-region than the high-elevation permafrost sub-region occurred across all four seasons, especially in spring. Increases in air temperature during the 1930s–1940s are apparent in the high-latitude permafrost sub-region, and although these increases are also seen in the high-elevation permafrost sub-region, they are comparatively relatively weak in amplitude. For the period

1979–2014, similar to the period of 1901–2014, there was a faster increase in air temperature in the high-latitude permafrost sub-region than in the high-elevation permafrost sub-region: a trend in the high-latitude permafrost sub-region of 0.40 °C decade⁻¹ (1.18 times larger than that in the high-elevation permafrost sub-region, with a value of 0.34 °C decade⁻¹). The NSE between CRU data and JRA-55 and ERA-Interim reanalysis data are 0.98 and 0.96, respectively, in the high-latitude permafrost sub-region, which indicates that CRU data are reliable within the high-latitude permafrost sub-region. Corresponding values of the NSE are 0.68 and 0.76 in the high-elevation permafrost sub-region. Although these values are somewhat close to 1, they are lower than those in the high-latitude permafrost sub-region, which indicates that CRU data are basically reliable in the high-elevation permafrost sub-region, but their performance is relatively low compared to that in the high-latitude permafrost

Table 1. Statistics of trends (°C decade^{-1}) in air temperature over all investigated permafrost regions.

	1901–2014	1979–2014	1998–2014	RCP4.5		RCP8.5	
				2006–2035	2006–2099	2006–2035	2006–2099
Entire region							
Annual	**0.13**	**0.39**	0.32	**0.44** ± 0.20	**0.35** ± 0.11	**0.59** ± 0.24	**0.78** ± 0.19
Spring	**0.17**	**0.48**	0.49	**0.38** ± 0.23	**0.32** ± 0.13	**0.54** ± 0.29	**0.70** ± 0.23
Summer	**0.08**	**0.33**	0.11	**0.36** ± 0.17	**0.25** ± 0.10	**0.41** ± 0.21	**0.59** ± 0.18
Autumn	**0.09**	**0.52**	0.53	**0.49** ± 0.22	**0.38** ± 0.10	**0.70** ± 0.24	**0.82** ± 0.17
Winter	**0.18**	0.15	0.06	**0.53** ± 0.32	**0.44** ± 0.14	**0.74** ± 0.32	**1.04** ± 0.24
High-latitude							
Annual	**0.13**	**0.40**	0.34	**0.44** ± 0.21	**0.35** ± 0.12	**0.59** ± 0.24	**0.79** ± 0.20
Spring	**0.18**	**0.49**	0.51	**0.38** ± 0.23	**0.32** ± 0.14	**0.54** ± 0.30	**0.70** ± 0.24
Summer	**0.09**	**0.33**	0.11	**0.36** ± 0.18	**0.25** ± 0.10	**0.41** ± 0.22	**0.59** ± 0.19
Autumn	**0.10**	**0.52**	**0.57**	**0.50** ± 0.22	**0.38** ± 0.11	**0.71** ± 0.25	**0.82** ± 0.18
Winter	**0.19**	0.14	0.08	**0.54** ± 0.33	**0.44** ± 0.14	**0.75** ± 0.32	**1.06** ± 0.24
High-elevation							
Annual	**0.08**	**0.34**	−0.22	**0.37** ± 0.17	**0.28** ± 0.07	**0.45** ± 0.17	**0.63** ± 0.13
Spring	**0.09**	**0.33**	−0.07	0.34 ± 0.21	**0.27** ± 0.09	**0.44** ± 0.22	**0.62** ± 0.15
Summer	**0.05**	**0.31**	0.05	**0.39** ± 0.18	**0.27** ± 0.06	**0.43** ± 0.13	**0.58** ± 0.10
Autumn	**0.06**	**0.33**	−0.39	**0.41** ± 0.20	**0.30** ± 0.08	**0.47** ± 0.20	**0.65** ± 0.12
Winter	**0.13**	**0.35**	−0.52	0.37 ± 0.24	**0.30** ± 0.09	**0.51** ± 0.27	**0.69** ± 0.18
Russia							
Annual	**0.14**	**0.45**	**0.94**	0.44 ± 0.26	**0.35** ± 0.12	**0.60** ± 0.28	**0.80** ± 0.22
Spring	**0.21**	**0.80**	**1.68**	0.38 ± 0.29	**0.32** ± 0.16	0.54 ± 0.35	**0.70** ± 0.28
Summer	**0.08**	**0.37**	0.17	**0.37** ± 0.21	**0.26** ± 0.11	**0.43** ± 0.26	**0.63** ± 0.21
Autumn	**0.10**	**0.60**	**1.48**	**0.53** ± 0.29	**0.40** ± 0.11	**0.73** ± 0.33	**0.85** ± 0.19
Winter	**0.17**	−0.16	0.24	0.51 ± 0.46	**0.41** ± 0.14	**0.75** ± 0.38	**1.04** ± 0.26
Canada							
Annual	**0.13**	**0.36**	−0.39	**0.45** ± 0.25	**0.36** ± 0.13	**0.59** ± 0.27	**0.81** ± 0.20
Spring	**0.14**	0.12	−0.92	0.39 ± 0.33	**0.33** ± 0.14	**0.56** ± 0.32	**0.71** ± 0.22
Summer	**0.10**	**0.28**	0.08	**0.35** ± 0.21	**0.23** ± 0.10	**0.37** ± 0.23	**0.56** ± 0.18
Autumn	**0.09**	**0.45**	−0.63	**0.47** ± 0.28	**0.39** ± 0.13	**0.73** ± 0.29	**0.83** ± 0.19
Winter	**0.21**	**0.51**	−0.24	0.57 ± 0.46	**0.51** ± 0.19	0.73 ± 0.42	**1.16** ± 0.28
Alaska							
Annual	**0.14**	0.25	−0.02	0.53 ± 0.32	**0.36** ± 0.12	**0.73** ± 0.38	**0.78** ± 0.20
Spring	**0.15**	−0.08	−0.81	0.48 ± 0.42	**0.32** ± 0.15	0.74 ± 0.39	**0.72** ± 0.22
Summer	**0.12**	**0.23**	0.06	0.42 ± 0.33	**0.25** ± 0.11	**0.50** ± 0.34	**0.57** ± 0.20
Autumn	**0.09**	**0.54**	0.31	0.51 ± 0.29	**0.35** ± 0.12	0.66 ± 0.45	**0.73** ± 0.18
Winter	**0.21**	0.38	0.86	0.74 ± 0.65	**0.51** ± 0.17	1.01 ± 0.76	**1.12** ± 0.28
Mongolia							
Annual	**0.18**	**0.31**	−0.57	**0.33** ± 0.20	**0.26** ± 0.08	**0.45** ± 0.20	**0.61** ± 0.17
Spring	**0.23**	**0.58**	−0.06	0.25 ± 0.28	**0.25** ± 0.11	0.35 ± 0.18	**0.59** ± 0.18
Summer	**0.08**	**0.53**	−0.59	**0.34** ± 0.19	**0.26** ± 0.09	**0.41** ± 0.16	**0.61** ± 0.17
Autumn	**0.15**	0.35	0.10	0.34 ± 0.23	**0.25** ± 0.09	**0.49** ± 0.32	**0.61** ± 0.15
Winter	**0.24**	−0.11	−1.26	0.46 ± 0.44	**0.27** ± 0.10	0.61 ± 0.33	**0.63** ± 0.19
China							
Annual	**0.10**	**0.31**	−0.24	**0.37** ± 0.16	**0.28** ± 0.07	**0.46** ± 0.15	**0.63** ± 0.13
Spring	**0.13**	**0.32**	−0.16	**0.32** ± 0.20	**0.26** ± 0.08	**0.42** ± 0.20	**0.60** ± 0.15
Summer	**0.05**	**0.33**	0.04	**0.38** ± 0.15	**0.26** ± 0.07	**0.43** ± 0.13	**0.58** ± 0.11
Autumn	**0.08**	**0.36**	−0.14	**0.40** ± 0.19	**0.29** ± 0.08	**0.49** ± 0.17	**0.65** ± 0.12
Winter	**0.16**	**0.20**	**−0.73**	0.38 ± 0.23	**0.29** ± 0.07	**0.52** ± 0.22	**0.70** ± 0.16

Bold numbers represents a statistical significance >95%; range of uncertainty is one standard deviation across models.

sub-region. It is considered that the lower NSE values may be attributed to sparse station observations in the permafrost region on the Tibetan Plateau (Guo and Wang, 2012; Guo *et al.*, 2016), which results in larger differences between CRU data (produced based on station observations only) and JRA-55 and ERA-Interim reanalysis data (produced based on station observations, satellite data, and model data). This in turn demonstrates the rationality of using state-of-the-art reanalysis data to evaluate the performance of CRU data in permafrost sub-regions.

Of the permafrost sub-regions in the five countries, Mongolia shows the largest increased trend in air temperature from 1901 to 2014, with a trend of 0.18 °C decade^{-1}, followed by Russia (0.14 °C decade^{-1}), Alaska (0.14 °C decade^{-1}), Canada (0.13 °C decade^{-1}), and China (0.10 °C decade^{-1}) (Figures 3(c)–(g)). These increases result from the largest increased trend in air temperature in Mongolia during spring, autumn, and winter (Table 1). Increases in air temperature during the 1930s–1940s are apparent in the permafrost sub-regions
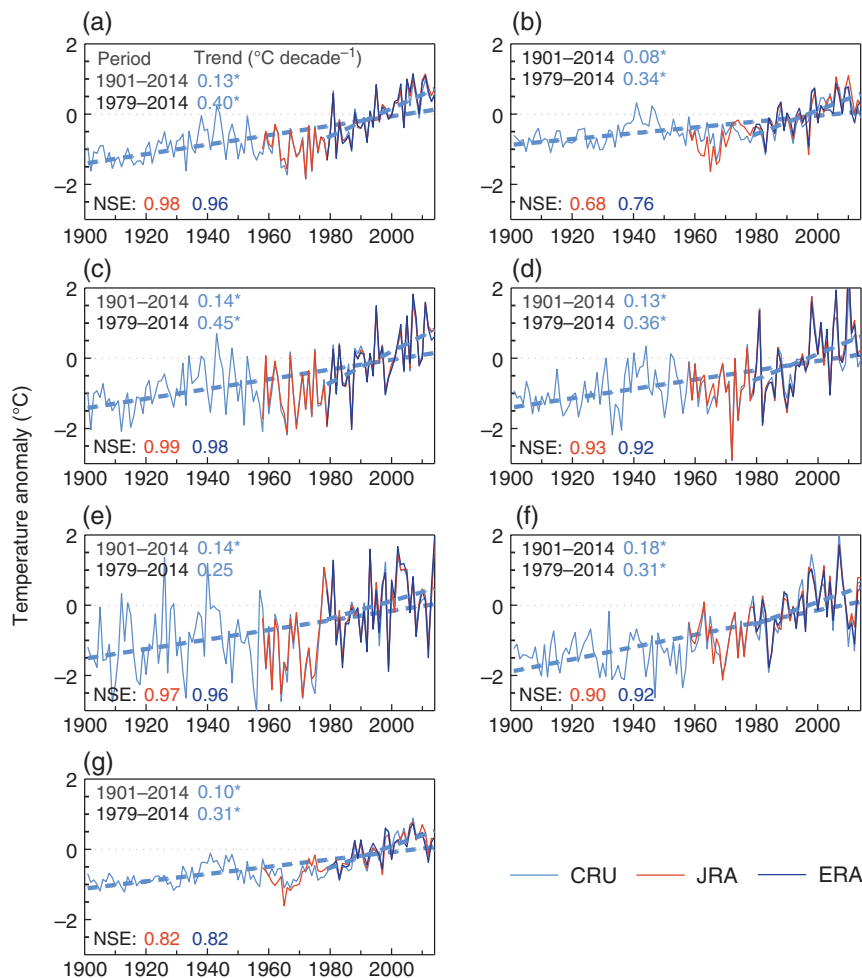
Figure 3. Changes in yearly temperature anomalies (relative to 1981–2010) in each permafrost sub-region, including: high-latitude (a) and high-elevation (b) permafrost sub-regions; and permafrost sub-regions in Russia (c), Canada (d), Alaska (e), Mongolia (f), and China (g), from CRU, JRA-55 (JRA), and ERA-Interim (ERA) data. Temperature trends (°C decade^{-1}) from CRU data and the corresponding periods in each permafrost sub-region are given in the top left corner of each panel, and * indicates that trends are significant at the 95% confidence level. The NSE is given in the lower left corner of each panel to show the similarity between the JRA-55 and ERA-Interim reanalysis and the CRU observations.

of Russia, Canada, and China, but are not apparent in the permafrost sub-regions of Mongolia and Alaska. For the period 1979–2014, the permafrost sub-region of Russia shows the largest increase in air temperature, with a trend 0.45 °C decade^{-1}, followed by Canada (0.36 °C decade^{-1}), Mongolia (0.31 °C decade^{-1}), China (0.31 °C decade^{-1}), and Alaska (0.25 °C decade^{-1}); this is a result of the largest increased trend in air temperature in Russia during spring and autumn (Table 1). The NSE between CRU data and JRA-55 reanalysis data are 0.99, 0.93, 0.97, 0.90, and 0.82 for permafrost sub-regions in Russia, Canada, Alaska, Mongolia, and China, respectively; and the NSE between the CRU data and ERA-Interim reanalysis data are 0.98, 0.92, 0.96, 0.92, and 0.82 for permafrost sub-regions in Russia, Canada, Alaska, Mongolia, and China, respectively. Notably, the NSE value in the permafrost sub-region in China is slightly lower than that in other countries; this is because most of the permafrost in China is located on the Tibetan Plateau, where station observations are sparse (particularly on the western Tibetan Plateau) (Guo and Wang, 2012; Guo *et al.*, 2016).

3.3. Comparison of warming between the permafrost region and globally

As shown in Figure 4, inter-annual variations in air temperature in the permafrost region are much more obvious than those occurring globally. The increase in air temperature in the permafrost region is 1.74 times more significant than the global level from 1901 to 2014. The rate of warming from 1979 to 2014 in the permafrost region was 2.50 times larger than that on a global level. Larger warming in the permafrost region than globally indicates that an even moderate global warming may have large implications for permafrost.

From 1998 to 2014, global mean air temperatures experienced weak warming, at a rate of warming of 0.06 °C decade^{-1} (not exceeding the 90% significance level), indicating a so-called 'global warming hiatus' relative to the significant warming during the previous period. However, the rate of warming in the permafrost region remained large from 1998 to 2014, at a value of 0.32 °C decade^{-1}, exceeding the 90% significance level. This indicates that the global warming hiatus did not
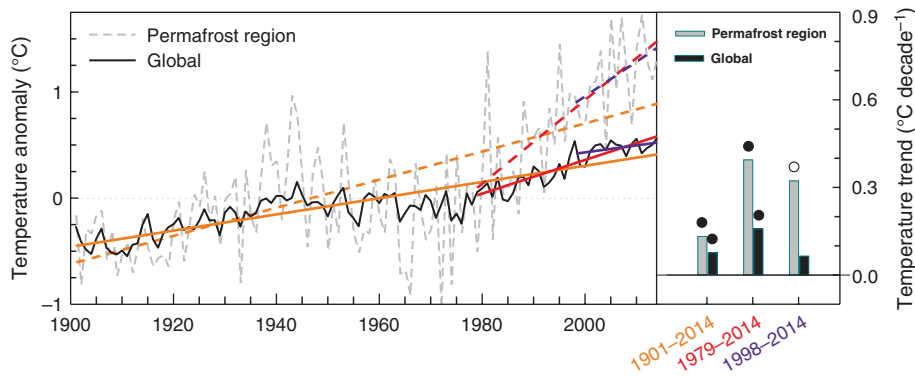
Figure 4. Comparison of anomalies (relative to 1961–1990) (left panel) and trends (right panel) in temperature in the permafrost region with the global level from HadCRUT4 data. Orange, red, and blue-dashed (solid) lines in the left panel represent regression lines of temperature anomalies in the permafrost (global) region for periods of 1901–2014, 1979–2014, and 1998–2014, respectively. Filled (open) circles in the right panel denote that the trend is significant at the 95% (90%) significance level.

occur in the permafrost region and implies that permafrost may continue to warm up despite the global warming. However, it should be considered that this recent and large warming rate in the permafrost region could include bias caused by poor weather station coverage, as explored in Cowtan and Way (2014).

4. Discussion

4.1. Uncertainty

Understanding climate change in the permafrost region is important for studying permafrost and its changes. This study presents the air temperature evolution in the permafrost region from CRU observations, which may be less accurate in the permafrost region due to the fewer observation stations, thereby causing large uncertainties in the results of the analysis presented in this study. To address this issue, two sets of state-of-the-art reanalysis data, the ERA-Interim and the JRA-55, are used to evaluate the suitability of CRU data in the permafrost region. Results show that CRU data closely match the two reanalysis datasets, indicating that CRU data are suitable for use in the permafrost region and that uncertainties in the analysis results are small. Despite this, the level of agreement between CRU data and reanalysis data is relatively low in the permafrost region of the Tibetan Plateau, indicating relatively larger uncertainties in the results in this area, which require further study and attention.

4.2. Comparison of historical and future air temperature evolution in permafrost regions

This study shows that yearly air temperatures in the entire permafrost region increased by $0.13\,°C\,decade^{-1}$ from 1901 to 2014 and $0.39\,°C\,decade^{-1}$ from 1979 to 2014. Future projections of yearly air temperature increase in the permafrost region are approximately 0.44 ± 0.20 (RCP4.5) and 0.59 ± 0.24 (RCP8.5) $°C\,decade^{-1}$ from 2006 to 2035 and 0.35 ± 0.11 (RCP4.5) and 0.78 ± 0.19 (RCP8.5) $°C\,decade^{-1}$ from 2006 to 2099

(Table 1). Seasonal warming occurred mostly during winter from 1901 to 2014 but during autumn from 1979 to 2014, while for future periods and scenarios it is forecast to occur uniformly mostly during winter.

This study also shows that air temperatures increased by 0.13, 0.08, 0.14, 0.13, 0.14, 0.18, and $0.10\,°C\,decade^{-1}$ in the high-latitude permafrost sub-region, the high-elevation permafrost sub-region, and Russia, Canada, Alaska, Mongolia, and China, respectively, from 1901 to 2014. In the future, mean air temperature will increase by 0.35 ± 0.12 (RCP4.5) or 0.79 ± 0.20 (RCP8.5) $°C\,decade^{-1}$ in the high-latitude permafrost sub-region; by 0.28 ± 0.07 (RCP4.5) or 0.63 ± 0.13 (RCP8.5) $°C\,decade^{-1}$ in the high-elevation permafrost sub-region; by 0.35 ± 0.12 (RCP4.5) or 0.80 ± 0.22 (RCP8.5) $°C\,decade^{-1}$ in the permafrost sub-region of Russia; by 0.36 ± 0.13 (RCP4.5) or 0.81 ± 0.20 (RCP8.5) $°C\,decade^{-1}$ in the permafrost sub-region of Canada; by 0.36 ± 0.12 (RCP4.5) or 0.78 ± 0.20 (RCP8.5) $°C\,decade^{-1}$ in the permafrost sub-region of Alaska; by 0.26 ± 0.08 (RCP4.5) or 0.61 ± 0.17 (RCP8.5) $°C\,decade^{-1}$ in the permafrost sub-region of Mongolia; and by 0.28 ± 0.07 (RCP4.5) or 0.63 ± 0.13 (RCP8.5) $°C\,decade^{-1}$ in the permafrost sub-region of China from 2006 to 2099 (Table 1). These results indicate that air temperatures may increase more significantly during the next 100 years for all investigated sub-regions of permafrost extent in the implementation of predictive models. Similar to the situation occurring during the historical period, warming in high-latitude permafrost sub-region is still predicted to be larger than that in high-elevation permafrost sub-region during two future periods (2006–2035 and 2006–2099). For the permafrost sub-regions in five countries, Mongolia showed the largest warming from 1901 to 2014, followed by Russia, Alaska, Canada, and China and Russia showed the largest warming from 1979 to 2014, followed by Canada, Mongolia, China, and Alaska, while Canada is predicted to experience the largest warming during the future period 2006–2099 under RCP85 scenario, followed by Russia, Alaska, China, and Mongolia.

4.3. Cause of increase in air temperature in permafrost region

The increase in air temperature in the permafrost region can be regarded as a regional response to global climate warming during the 20th century, and is mostly considered to be related to the positive uptake of energy by the climate system caused by radiative forcing of anthropogenic greenhouse gases emissions (IPCC, 2013). This study shows that the increase in air temperature in the permafrost region is 1.74 times greater than that occurring globally from 1901 to 2014. In addition, the increase in air temperature in the permafrost region is predicted to be 2.02 times greater than that occurring globally from 2006 to 2100 under the RCP4.5 scenario (Collins *et al.*, 2013; Slater and Lawrence, 2013). The permafrost region is mainly located in the northern high latitudes, and thus the larger increases in air temperature in this region may be a part of the so-called Arctic amplification of global climate warming (Serreze and Barry, 2011). The reasons for the greater increases in air temperature in the permafrost region may be similar to the cause of Arctic amplification. Previous studies indicate that ice and snow cover albedo feedback reduces upward shortwave radiation, and thus is responsible for the Arctic amplification (Serreze and Francis, 2006). Losses in sea ice cover alter vertical heat fluxes between the Arctic Ocean and the atmosphere, and further contribute to Arctic amplification (Serreze *et al.*, 2009). Changes in water vapour and cloud cover are also found to account for part of the polar amplification, by affecting downward longwave radiation fluxes at the surface (Francis and Hunter, 2006). Other reasons are related to soot on snow, which is linked to the burning of fossil fuels (Hansen and Nazarenko, 2004), and an increase in black carbon aerosol concentrations in the atmosphere (Shindell and Faluvegi, 2009). However, it is considered that each of these factors noted above is not singularly responsible, and that, usually, a combination of them has resulted in Arctic amplification.

5. Summary

Historical air temperature evolution in the permafrost region is investigated based on CRU data in combination with JRA-55 and ERA-Interim reanalysis data. Yearly air temperatures increased by 0.13 (0.39) °C decade⁻¹ from 1901 to 2014 (1979–2014). Winter (autumn) showed the largest increase in air temperature compared to the other three seasons from 1901 to 2014 (1979–2014). The high-latitude permafrost sub-region experienced an increase in air temperature 1.63 (1.18) times greater than that occurring in the high-elevation permafrost sub-region for 1901–2014 (1979–2014). Out of the permafrost sub-regions in different countries, Mongolia showed the highest increase in air temperature from 1901 to 2014, followed by Russia, Alaska, Canada, and China, while Russia showed the highest increase in air temperature from 1979 to 2014, followed by Canada, Mongolia, China, and Alaska. Relative to the global situation, the air temperature evolution in the permafrost region had a larger inter-annual variation, a more increase of 1.74 (2.50) times from 1901 to 2014 (1979–2014), and a significant increase even during the global warming hiatus period from 1998 to 2014. This indicates that an even moderate global warming may have a large implication for permafrost. In addition, relative to historical warming and based on predictive models, a more significant increase in air temperature will occur during the next 100 years for all the investigated permafrost regions.

The results of this study provide detailed information and analyses with respect to climate change in the permafrost region, which can serve as a basis for further research in both permafrost and climate communities. The evaluation of uncertainties, based on JRA-55 and ERA-Interim reanalysis data, indicates small uncertainties in the results. Our datasets are available from the authors to members of both permafrost and climate communities in order to help with various corresponding studies, such as modelling efforts on permafrost. Air temperature change is the most important factor inducing permafrost change (Muller, 1947), and therefore, this study investigates its historical evolution. However, changes in precipitation (snow) and radiation may also effect permafrost change to some extent (Koven *et al.*, 2013), and therefore, future studies will focus on changes in precipitation and radiation within the permafrost region during historical and future periods.

This study also shows that air temperatures in the permafrost region experienced a significant increase during (approximately) the 1930s–1940s. Further work will also focus on investigating the response of permafrost to this temporary increase in air temperature, which will be useful in understanding the question of what level of increase in air temperature produces permafrost thawing.

References

Anisimov OA, Nelson FE. 1996. Permafrost distribution in the Northern Hemisphere under scenarios of climate change. *Glob. Planet. Change* **14**: 59–72.

Anisimov OA, Reneva S. 2006. Permafrost and changing climate: the Russian perspective. *AMBIO* **35**: 169–175.

Blunden J, Arndt DS (eds). 2016. State of the climate in 2015. *Bull. Am. Meteorol. Soc.* **97**: S1–S275.

Brown J, Ferrians Jr OJ, Heginbottom JA, Melnikov ES. 1997. *Circum-Arctic Map of Permafrost and Ground-Ice Conditions*, US Geological Survey in Cooperation with the Circum-Pacific Council for Energy and Mineral Resources, Circum-Pacific Map Series CP-45, scale 1:10,000,000, 1 sheet.

Brown J, Hinkel K, Nelson F. 2000. The circumpolar active layer monitoring (CALM) program: research designs and initial results. *Polar Geogr.* **24**: 165–258.

Burke EJ, Jones CD, Koven CD. 2013. Estimating the permafrost-carbon climate response in the CMIP5 climate models using a simplified approach. *J. Clim.* **26**: 4897–4909.

Callaghan TV, Johansson M, Anisimov O, Christiansen HH, Instanes A, Romanovsky V, Smith S. 2012. Changing permafrost and its impacts. In *Snow, Water, Ice and Permafrost in the Arctic (SWIPA)*. Arctic Monitoring and Assessment Program (AMAP): Oslo.

Cheng GD, Wang SL. 1982. On the zonation of high-altitude permafrost in China (in Chinese). *J. Glaciol. Geocryol.* **4**: 1–17.

Christiansen HH, Etzelmuller B, Isaken K, Juliussen H, Farbot H, Humlum O, Johansson M, Ingeman-Neilsen T, Kristensen L, Hjort J, Holmlund P, Sannel ABK, Sigsgaard C, Akerman J, Foged N, Blikra LH, Pernosky MA, Odegard R. 2010. Thermal state of permafrost in the Nordic area during the IPY 2007-2009. *Permafr. Periglac. Process.* **21**: 156–181.

Collins M, Knutti R, Arblaster J, Dufresne JL, Fichefet T, Friedlingstein P, Gao X, Gutowski WJ, Johns T, Krinner G, Shongwe M, Tebaldi C, Weaver AJ, Wehner M. 2013. Long-term climate change: projections, commitments and irreversibility. In *Climate Change 2013: The Physical Science Basis. Contribution of Working Group I to the Fifth Assessment Report of the Intergovernmental Panel on Climate Change*, Stocker TF, Qin D, Plattner GK, Tignor M, Allen SK, Boschung J, Nauels A, Xia Y, Bex V, Midgley PM (eds). Cambridge University Press: Cambridge, UK and New York, NY.

Cowtan K, Way RG. 2014. Coverage bias in the HadCRUT4 temperature series and its impact on recent temperature trends. *Q. J. R. Meteorol. Soc.* **140**: 1935–1944.

Dee DP, Uppala SM, Simmons AJ, Berrisford P, Poli P, Kobayashi S, Andrae U, Balmaseda MA, Balsamo G, Bauer P, Bechtold P, Beljaars ACM, Berg L, Bidlot J, Bormann N, Delsol C, Dragani R, Fuentes M, Geer AJ, Haimberger L, Healy SB, Hersbach H, Hólm EV, Isaksen L, Kållberg P, Köhler M, Matricardi M, McNally AP, Monge-Sanz BM, Morcrette JJ, Park BK, Peubey C, Rosnay P, Tavolato C, Thépaut JN, Vitart F. 2011. The ERA-Interim reanalysis: configuration and performance of the data assimilation system. *Q. J. R. Meteorol. Soc.* **137**: 553–597.

Derksen C, Smith SL, Sharp M, Brown L, Howell S, Copland L, Mueller DR, Gauthier Y, Fletcher C, Tivy A, Bernier M, Bourgeois J, Brown R, Burn CR, Duguay C, Kushner P, Langlois A, Lewkowicz AG, Royer A, Walker A. 2012. Variability and change in the Canadian cryosphere. *Clim. Change* **115**: 59–88.

Francis JA, Hunter E. 2006. New insight into the disappearing Arctic sea ice. *EOS Trans. Am. Geophys. Union* **87**: 509–511.

Guo DL, Sun JQ. 2015. Permafrost thaw and associated settlement hazard onset timing over the Qinghai-Tibet engineering corridor. *Int. J. Disaster Risk Sci.* **6**: 347–358.

Guo DL, Wang HJ. 2012. The significant climate warming in the northern Tibetan Plateau and its possible causes. *Int. J. Climatol.* **32**: 1775–1781.

Guo DL, Wang HJ. 2013. Simulation of permafrost and seasonally frozen ground conditions on the Tibetan Plateau, 1981-2010. *J. Geophys. Res. Atmos.* **118**: 5216–5230.

Guo DL, Wang HJ. 2014. Simulated change in the near-surface soil freeze/thaw cycle on the Tibetan Plateau from 1981 to 2010. *Chin. Sci. Bull.* **59**: 2439–2448.

Guo DL, Wang HJ. 2016a. CMIP5 permafrost degradation projection: a comparison among different regions. *J. Geophys. Res. Atmos.* **121**: 4499–4517.

Guo DL, Wang HJ. 2016b. Permafrost degradation and associated ground settlement estimation under 2°C global warming. *Clim. Dyn.* https://doi.org/10.1007/s00382-016-3469-9.

Guo DL, Yang MX, Wang HJ. 2011a. Characteristics of land surface heat and water exchange under different soil freeze/thaw conditions over the central Tibetan Plateau. *Hydrol. Process.* **25**: 2531–2541.

Guo DL, Yang MX, Wang HJ. 2011b. Sensible and latent heat flux response to diurnal variation in soil surface temperature and moisture under different freeze/thaw soil conditions in the seasonal frozen soil region of the central Tibetan Plateau. *Environ. Earth Sci.* **63**: 97–107.

Guo DL, Wang HJ, Li D. 2012. A projection of permafrost degradation on the Tibetan Plateau during the 21st century. *J. Geophys. Res.* **117**: D05106. https://doi.org/10.1029/2011JD016545.

Guo DL, Yu ET, Wang HJ. 2016. Will the Tibetan Plateau warming depend on elevation in the future? *J. Geophys. Res. Atmos.* **121**: 3969–3978.

Hansen J, Nazarenko L. 2004. Soot climate forcing via snow and ice albedo. *Proc. Natl. Acad. Sci.* **101**: 423–428.

Harris C, Isaksen K. 2008. Recent warming of European permafrost: evidence from borehole monitoring. In *Proceedings of the Ninth International Conference on Permafrost*, Kane DL, Hinkel KM (eds). Institute of Northern Engineering, University of Alaska Fairbanks, Fairbanks, vol. 1, 655–661.

Harris I, Jones PD, Osborn TJ, Lister DH. 2014. Updated high-resolution grids of monthly climatic observations – the CRU TS3. 10 Dataset. *Int. J. Climatol.* **34**: 623–642.

Hartmann DL, Klein Tank AMG, Rusticucci M, Alexander LV, Brönnimann S, Charabi Y, Dentener FJ, Dlugokencky EJ, Easterling DR, Kaplan A, Soden BJ, Thorne PW, Wild M, Zhai PM. 2013. Observations: atmosphere and surface. In *Climate Change 2013: The Physical Science Basis. Contribution of Working Group I to the Fifth Assessment Report of the Intergovernmental Panel on Climate Change*, Stocker TF, Qin D, Plattner G-K, Tignor M, Allen SK, Boschung J, Nauels A, Xia Y, Bex V, Midgley PM (eds). Cambridge University Press: Cambridge, UK and New York, NY.

IPCC. 2013. Summary for policymakers. In *Climate Change 2013: The Physical Science Basis. Contribution of Working Group I to the Fifth Assessment Report of the Intergovernmental Panel on Climate Change*, Stocker TF, Qin D, Plattner G-K, Tignor M, Allen SK, Boschung J, Nauels A, Xia Y, Bex V, Midgley PM (eds). Cambridge University Press: Cambridge, UK and New York, NY.

Jones PD, Lister DH, Osborn TJ, Harpham C, Salmon M, Morice CP. 2012. Hemispheric and large-scale land surface air temperature variations: an extensive revision and an update to 2010. *J. Geophys. Res.* **117**: D05127. https://doi.org/10.1029/2011JD017139.

Kobayashi C, Iwasaki T. 2016. Brewer-Dobson circulation diagnosed from JRA-55. *J. Geophys. Res. Atmos.* **121**: 1493–1510.

Kobayashi S, Ota Y, Harada Y, Ebita A, Moriya M, Onoda H, Onogi K, Kamahori H, Kobayashi C, Endo H, Miyaoka K, Takahashi K. 2015. The JRA-55 reanalysis: general specifications and basic characteristics. *J. Meteorol. Soc. Jpn.* **93**: 5–48.

Koven CD, Ringeval B, Friedlingstein P, Ciais P, Cadule P, Khvorostyanov D, Krinner G, Tarnocai C. 2011. Permafrost carbon-climate feedbacks accelerate global warming. *Proc. Natl. Acad. Sci.* **108**: 14769–14774.

Koven CD, Riley WJ, Stern A. 2013. Analysis of permafrost thermal dynamics and response to climate change in the CMIP5 earth system models. *J. Clim.* **26**: 1877–1900.

Koven CD, Schuur EAG, Schädel C, Bohn TJ, Burke EJ, Chen G, Chen X, Ciais P, Grosse G, Harden JW, Hayes DJ, Hugelius G, Jafarov EE, Krinner G, Kuhry P, Lawrence DM, MacDougall AH, Marchenko SS, McGuire AD, Natali SM, Nicolsky DJ, Olefeldt D, Peng S, Romanovsky VE, Schaefer KM, Strauss J, Treat CC, Turetsky M. 2015. A simplified, data-constrained approach to estimate the permafrost carbon-climate feedback. *Phil. Trans. R. Soc. A* **373**: 20140423.

Lan C, Zhang YX, Bohn TJ, Zhao L, Li JL, Liu QM, Zhou BR. 2015. Frozen soil degradation and its effects on surface hydrology in the northern Tibetan Plateau. *J. Geophys. Res. Atmos.* **120**: 8276–8298.

Lawrence DM, Slater AG. 2005. A projection of severe near-surface permafrost degradation during the 21st century. *Geophys. Res. Lett.* **32**: L24401. https://doi.org/10.1029/2005GL025080.

Lawrence DM, Slater AG, Swenson SC. 2012. Simulation of present-day and future permafrost and seasonally frozen ground conditions in CCSM4. *J. Clim.* **25**: 2207–2225.

Li Q, Chen HS. 2013. Variation of seasonal frozen soil in east China and their association with monsoon activity under the background of global warming (in Chinese). *Clim. Change Res. Lett.* **2**: 47–53.

Liljedahl AK, Boike J, Daanen RP, Fedorov AN, Frost GV, Grosse G, Hinzman LD, Iijma Y, Jorgenson JC, Matveyeva N, Necsoiu M, Raynolds MK, Romanovsky VE, Schulla J, Tape KD, Walker DA, Wilson CJ, Yabuki H, Zona D. 2016. Pan-Arctic ice-wedge degradation in warming permafrost and its influence on tundra hydrology. *Nat. Geosci.* **9**: 312–318.

Muller SW. 1947. *Permafrost or Permanently Frozen Ground and Related Engineering Problems*. J.W. Edwards: Ann Arbor, MI, 231.

Nash JE, Sutcliffe JV. 1970. River flow forecasting through conceptual models. Part I: a discussion of principles. *J. Hydrol.* **10**: 282–290.

Nelson FE, Anisimov OA, Shiklomanov NI. 2001. Subsidence risk from thawing permafrost. *Nature* **410**: 889–890.

Nelson FE, Anisimov OA, Shiklomanov N. 2002. Climate change and hazard zonation in the circum-Arctic permafrost regions. *Nat. Hazards* **26**: 203–225.

Ngo-Duc T, Tangang FT, Santisirisomboon J, Cruz F, Trinh-Tuan L, Nguyen-Xuan T, Phan-Van T, Juneng L, Narisma G, Singhruck P, Gunawan D, Aldrian E. 2016. Performance evaluation of RegCM4 in simulating extreme rainfall and temperature indices over the CORDEX-southeast Asia region. *Int. J. Climatol.* **37**: 1634–1647. https://doi.org/10.1002/joc.4803.

Noetzli J, Christiansen HH, Guglielmin M, Romanovsky VE, Shiklomanov NI, Smith SL, Zhao L. 2016. [Global climate] Permafrost thermal state [in "State of the climate in 2015"]. *Bull. Am. Meteorol. Soc.* **97**: S20–S22.

Peterson TC, Karl TR, Jamason PF, Knight R, Easterling DR. 1998. The first difference method: maximizing station density for the calculation of long-term global temperature change. *J. Geophys. Res.* **103**: 25967–25974.

Qin DH, Zhou BT, Xiao CD. 2014. Progress in studies of cryospheric changes and their impacts on climate of China. *J. Meteorol. Res.* **28**: 732–746.

Romanovsky VE, Smith SL, Christiansen HH. 2010a. Permafrost thermal state in the polar Northern Hemisphere during the international polar year 2007–2009: a synthesis. *Permafr. Periglac. Process.* **21**: 106–116.

Romanovsky VE, Drozdov DS, Oberman NG, Malkova GV, Kholodov AL, Marchenko SS, Moskalenko NG, Sergeev DO, Ukrainsteva DG, Abramov AA, Vasiliev AA. 2010b. Thermal state of permafrost in Russia. *Permafr. Periglac. Process.* **21**: 136–155.

Romanovsky VE, Smith SL, Isaksen K, Shiklomanov NI, Streletskiy DA, Kholodov AL, Christiansen HH, Drozdov DS, Malkova GV, Marchenko SS. 2016. [Arctic] Terrestrial permafrost [in "State of the climate in 2015"]. *Bull. Am. Meteorol. Soc.* **97**: S149–S152.

Schuur E, Vogel J, Crummer K, Lee H, Sickman J, Osterkamp T. 2009. The effect of permafrost thaw on old carbon release and net carbon exchange from tundra. *Nature* **459**: 556–559.

Schuur E, McGuire AD, Schädel C, Grosse G, Harden JW, Hayes DJ, Hugelius G, Koven CD, Kuhry P, Lawrence DM, Natali SM, Olefeldt D, Romanovsky VE, Schaefer K, Turetsky MR, Treat CC, Vonk JE. 2015. Climate change and the permafrost carbon feedback. *Nature* **520**: 171–179.

Serreze MC, Barry RG. 2011. Processes and impacts of Arctic amplification: a research synthesis. *Glob. Planet. Change* **77**: 85–96.

Serreze MC, Francis JA. 2006. The Arctic amplification debate. *Clim. Change* **76**: 241–264.

Serreze MC, Barrett AP, Stroeve JC, Kindig DM, Holland MM. 2009. The emergence of surface-based Arctic amplification. *Cryosphere* **3**: 11–19.

Shiklomanov NI, Streletskiy DA, Nelson FE. 2012. Northern Hemisphere component of the global circumpolar active layer monitoring (CALM) program. In *Proceedings of the 10th International Conference on Permafrost*, Salekhard, Russia, 25–29 June, vol. 1, 377–382.

Shindell D, Faluvegi G. 2009. Climate response to regional radiative forcing during the twentieth century. *Nat. Geosci.* **2**: 294–300.

Simmons AJ, Jones PD, da Costa BV, Belijaars ACM, Kallberg PW, Saarinen S, Uppala SM, Viterbo P, Wedi N. 2004. Comparison of trends and low-frequency variability in CRU, ERA-40, and NCEP/NCAR analyses of surface air temperature. *J. Geophys. Res.* **109**: D24115. https://doi.org/10.1029/2004JD005306.

Slater AG, Lawrence DM. 2013. Diagnosing present and future permafrost from climate models. *J. Clim.* **26**: 5608–5623.

Smith SL, Romanovsky VE, Lewkowicz AG, Burn CR, Allard M, Clow GD, Yoshikawa K, Throop J. 2010. Thermal state of permafrost in North America: a contribution to the international polar year. *Permafr. Periglac. Process.* **21**: 117–135.

Smith SL, Throop J, Lewkowicz AG. 2012. Recent changes in climate and permafrost temperatures at forested and polar desert sites in northern Canada. *Can. J. Earth Sci.* **49**: 914–924.

Stendel M, Christensen J. 2002. Impact of global warming on permafrost conditions in a coupled GCM. *Geophys. Res. Lett.* **29**: 1632. https://doi.org/10.1029/2001GL014345.

Sylla MB, Coppola E, Mariotti L, Giorgi F, Ruti PM, Dell'Aquila A, Bi X. 2010. Multiyear simulation of the African climate using a regional climate model (RegCM3) with the high resolution ERA-Interim reanalysis. *Clim. Dyn.* **35**: 231–247.

Taylor KE, Stouffer RJ, Meehl GA. 2012. An overview of CMIP5 and the experiment design. *Bull. Amer. Meteor. Soc.* **93**: 485–498.

Throop J, Lewkowicz AG, Smith SL. 2012. Climate and ground temperature relations at sites across the continuous and discontinuous permafrost zones, northern Canada. *Can. J. Earth Sci.* **49**: 865–876.

Wang A, Zeng X. 2012. Evaluation of multi-reanalysis products with *in situ* observations over the Tibetan Plateau. *J. Geophys. Res. Atmos.* **117**: D05102. https://doi.org/10.1029/2011JD016553.

Way RG, Bonnaventure PP. 2015. Testing a reanalysis-based infilling method for areas with sparse discontinuous air temperature data in northeastern Canada. *Atmos. Sci. Lett.* **16**: 398–407.

Wu J, Gao XJ. 2013. A gridded daily observation dataset over China region and comparison with the other datasets. *Chin. J. Geophys.* **56**: 1102–1111.

Wu QB, Zhang TJ. 2008. Recent permafrost warming on the Qinghai-Tibetan Plateau. *J. Geophys. Res.* **113**: D13108. https://doi.org/10.1029/2007JD009539.

Yanase W, Niino H, Watanabe SI, Hodges K, Zahn M, Spengler T, Gurvich I. 2016. Climatology of polar lows over the Sea of Japan using the JRA-55 reanalysis. *J. Clim.* **29**: 419–437.

Yang MX, Nelson F, Shiklomanov N, Guo DL, Wan G. 2010. Permafrost degradation and its environmental effects on the Tibetan Plateau: a review of recent research. *Earth Sci. Rev.* **103**: 31–44.

Zhang T, Barry RG, Knowles K, Heginbottom JA, Brown J. 1999. Statistics and characteristic of permafrost and ground-ice distribution in the Northern Hemisphere. *Polar Geogr.* **23**: 132–154.

Zhao L, Wu QB, Marchenko SS, Sharkhuu N. 2010. Thermal state of permafrost and active layer in central Asia during the international polar year. *Permafr. Periglac. Process.* **21**: 198–207.

Zhou BT, Xu Y, Wu J, Dong S, Shi Y. 2016. Changes in temperature and precipitation extreme indices over China: analysis of a high-resolution grid dataset. *Int. J. Climatol.* **36**: 1051–1066.

Zimov S, Schuur E, Chapin F III. 2006. Permafrost and the global carbon budget. *Science* **312**: 1612–1613.